Conference on Modelling Fluid Flow (CMFF'25)
The 19th International Conference on Fluid Flow Technologies
Budapest, Hungary, August 26 - August 29, 2025

HAZARD PREDICTION MODELS FOR BATTERY MODULE AND PACKS: FLAMMABILITY, PARTICLE IGNITED VENT GAS, ARCING WITHOUT AND WITH PARTICLES

Thirumalesha Chittipotula[1], Lucas Eder[2], David Schellander[3]

[1] Corresponding Author. AVL List GmbH, Hans-List-Platz 1, 8020 Graz, Austria, Email: thirumalesha.chittipotula@avl.com
[2] AVL List GmbH, Hans-List-Platz 1, 8020 Graz, Austria, Email: lucas.eder@avl.com
[3] AVL List GmbH, Hans-List-Platz 1, 8020 Graz, Austria, Email: david.schellander@avl.com

ABSTRACT

The safety of the battery cells, module and the pack is very important for the overall safety of an electric vehicle. In this context, "thermal runaway" and "arcing" are two phenomena that require special focus. The current study focuses on predictive modelling of flammability, ignition and arcing in battery module and packs by considering several vent gas species and particles ejected during the battery thermal runaway. Considering the wide range of vent gas species and their compositions, a methodology is developed to incorporate these species in the evaluation of the overall flammability, breakdown voltage and arc-generating capability. Furthermore, a method is presented for modelling the "particle ignited vent gas" and "influence of particles on arcing". The vent gas combustion (with particles as an ignition source) is modelled using two different skeleton mechanisms consisting of various flammable vent gas species. These models are incorporated in a 3D CFD solver (AVL FIRE™ M). The simulations are first performed on simple geometries and later expanded to a full battery pack (consisting of several modules) providing significant insights into the safety of the overall battery system.

Keywords: Arc-generating capability, Breakdown voltage, Hazard prediction, Flammability, Particle ignited vent gas

NOMENCLATURE

A	[1/(Pa m)]	saturation ionization
B	[V/(Pa m)]	ionization energy
D	[m^2/s]	effective diffusivity
E	[V/m]	electrical field strength
F	[*N*]	force
LFL	[-]	lower flammability limit
LOC	[*N*]	limiting oxygen concentration
Q	[C]	electrical charge
UFL	[-]	upper flammability limit
V	[V]	voltage
d	[m]	distance
h	[J]	enthalpy
p	[*Pa*]	pressure
r	[*m*]	radius
t	[*s*]	time
x	[m]	cartesian point
y	[-]	vent gas species mass fraction
γ	[W/(mK)]	thermal conductivity
γ	[-]	emission coef.
ε	[F/m]	dielectric coef.
ρ	[kg/m^3]	density
τ	[N/m^2]	stress tensor
ω	[kg/s]	species source

Subscripts and Superscripts

B	breakdown
i	cartesian coordinate or species
j	cartesian coordinate or species
l	species
mix	mixture
p	particle
se	secondary electron

1. INTRODUCTION AND LITERATURE REVIEW

The safety of the battery module and the battery pack is of utmost importance for the overall safety of an electric vehicle. In this context, "flammability" and "arcing" are two important phenomena that require a special research focus.

The exact determination of the flammability limits in the battery packs is very important in connection with the venting of one or more battery cells, which poses the risk of destruction of the

battery pack and vehicle. In the past, the flammability prediction models are solely based on the pure components of the flammable gases. However, the vent gas from a battery cell consists of a mixture of flammable gases such as CH_4, C_2H_4, CO, and H_2 [1,2]. Depending on the battery material, the molar or the mass fractions of these gases may vary from moderate to high level. Some of these gases have a narrow flammability range, e.g., CH_4, while others have a wide flammability range, e.g., H_2 [2,3]. Therefore, in addition to pure component flammability limits, it is necessary to consider the mixture flammability limits in the battery domain. The mixture based flammable limits change spatially in the battery packs as the gas composition changes. These mixture limits are estimated efficiently in the computational domain while satisfying the thermodynamic principles of mixing [4,5]

Arcing involves the ionization and the electric discharge from the gas medium caused by a high voltage difference between the electrodes where the gas medium acts as the electrical conductor [6][7] . The temperatures in the low-current arcing are around 6500 K and can go up to 20000 K for high-current arcing. Such high temperatures can ignite an ignitable gas mixture and cause damage to battery cells and surrounding materials [8]. In battery packs there are several parts with different electrical potentials. The distances between the parts in modern batteries are very small, down to mm, to get high power density of the battery pack. For modelling the arcing between small gaps Paschen's law is commonly used [9,10], which defines that the gap distance and the pressure in the gap both influence the arcing possibility and must be considered together for getting the breakdown voltage. However, the parameters in the Paschen's law (Townsend constants) depend on the gas medium [10]. The aim of the current work is to accurately model the arc-related properties of battery modules and packs, taking real-world conditions into account (vent gas composition and the real electrode distances). The measured breakdown voltage and critical distances provide the user with the hazard limits to avoid potential arcing in the battery modules and packs. During thermal runaway and destruction of battery, particles can be generated. If particles are emitted into gaps between electrodes, they influence the arc-generating capability. In the gap particles can lead to micro discharge arcs and significantly reduce breakdown voltage [11]. Hence, if particles are in the gap, they should be considered in the computation of the breakdown voltage [12,13].

Furthermore, particles exerted from the venting process often have high temperatures and can ignite the combustible vent gas [14]. In the presence of oxygen and an ignition source this vent gas may ignite and cause rapid fires in the battery pack [15]. Therefore, in this study a model is implemented to incorporate the "particles as ignition source" and subsequent combustion of venting gas is presented.

2. GOVERNING EQUATIONS AND MODEL DESCRIPTION

The governing equations of the 3D CFD and thermal runaway kinetic solvers [16] along with the flammability, breakdown voltage and arcing related models.

3D-CFD Solver governing equations

Continuity, momentum and the enthalpy transport equations which are integral part of the CFD solver are described below.

$$\frac{\partial \rho}{\partial t} + \frac{\partial \rho\, v_j}{\partial x_j} = 0 \tag{1}$$

$$\frac{\partial \rho\, v_i}{\partial t} + \frac{\partial \rho\, v_i\, v_j}{\partial x_j} = -\frac{\partial P}{\partial x_i} + \frac{\partial \tau_{ij}}{\partial x_j} + F \tag{2}$$

$$\frac{\partial h}{\partial t} + \frac{\partial \rho\, v_j\, h}{\partial x_j} = \frac{\partial^2 \gamma\, h}{\partial {x_j}^2} + \dot{q} \tag{3}$$

$$\frac{\partial y_i}{\partial t} + \frac{\partial \rho\, v_j\, y_i}{\partial x_j} = \frac{\partial^2 Đ\, y_i}{\partial {x_j}^2} + \dot{\omega}_\iota \tag{4}$$

Where, ρ is density, v is velocity, P is pressure, τ_{ij} is stress tensor and F is additional forces (e.g., body force). Furthermore, h is the enthalpy of the system, x_j is cartesian component and γ is thermal conductivity. The second term in (3) represents the enthalpy transfer due to convection ($\rho\, v_j$) and is not applicable when applied to the solid domains. y_i is the vent gas species mass fraction in the fluid domain and $\dot{\omega}_\iota$ is the species source generated from the reaction due combustion of vent gas species. Here, Đ is the effective diffusivity of the vent gas species *i* with respect to all other species in the mixture of the venting gas. Effective diffusivity is evaluated as the averaged value based on the molar fractions of the species in the mixture.

The particles are modelled with the Lagrangian approach following [17] and literature cited therein. For particle-wall interaction the solid particle wall contact model including heat-transfer exchange between particles and walls is used.

Flammability

As the vent gas consists of several flammable gases, in this study a mixture flammability index is evaluated based on Le Chatelier's principle and the limiting oxygen concentration (LOC) as shown below [3,4].

$$LFL_{mix} = \frac{\sum y_i}{\sum LFL_i \, y_i} \quad (5)$$

$$UFL_{mix} = \frac{\sum y_i}{\sum UFL_i \, y_i} \quad (6)$$

$$LOC_{mix} = \frac{\sum y_i \, R_i}{\sum LOC_i \, y_i} \quad (7)$$

Where, *i* is flammable gases considered in the evaluation, LFL_i, UFL_i are the lower and upper flammable limits (LFL and UFL) of the pure components. LFL_{mix}, UFL_{mix} are the lower and upper flammability limits of the mixture. LOC_{mix} is the mixture limiting oxygen concentration and Ri is the stoichiometric molar ratio of oxygen to fuel. These flammability limits are determined experimentally for pure component fuels for e.g., Zlochower and Green [3]

The mixture flammability is evaluated in the similar lines as the pure component flammability is evaluated. Where, a parabolic function (flammability) generated from the molar fractions and the flammability limits of the respective components is used to predict the instantaneous values. In case of mixture, the parabolic function is generated based on the mixture molar mass and the mixture flammability limits (low and upper), described from Eqs. (5)-(6). Equation (7) provides an additional condition for the flammability index accounting the minimum oxygen requirement. Below this oxygen available limit the flammability index is set to 0. In the evaluation of the flammability limits several flammable gases produced during the battery thermal runaway such as CH_4, C_2H_4, C_2H_6, C_3H_8, C_4H_{10}, CO, and H_2 are included in this study.

Particle ignited vent gas

Several of FIRE M CFD solver modelling capabilities are combined for this application, such as spray (solid particles) and general gas phase reactions, where particle temperature in a cell acts as an ignition source. This model combination has been proved helpful in understanding the combustion of the vent gas. For modelling the combustion of vent gas mixture, a few reaction mechanisms are reduced from the GRI mechanism [18] by including all the important vent gas species. These reduced skeleton mechanisms (for e.g., consisting of 19 species and 41 reactions or consisting of 25 species and 100 reactions) can predict the initiation and propagation of the combustion in the battery packs in much faster simulation times than compared with the original mechanism. No turbulence chemistry interactions are considered in this study as the effects are not that significant due to the fact that the system is closed, non-moving, and limited in the oxygen concentration. The simulation results provide significant insights into understanding the hazard posed by the vent gas mixture in the presence of hot particles in the battery pack as shown latter in the results and discussion.

Breakdown voltage and Arcing

The prediction of breakdown voltage for pure component gases is straight forward from Paschen's law. The breakdown voltage depends on several factors such as electrode surfaces, terminal voltage, distance and the pressure of the gas medium between the electrodes.

$$V_B = \frac{B \, p \, d}{(\ln(A \, p \, d) - \ln(\ln(1 + \frac{1}{\gamma_{se}})))} \quad (8)$$

Where, V_B is the breakdown voltage p is pressure and d is distance between the electrodes and γ_{se} is the secondary electron emission coefficient and A, B are Townsend's coefficients. A mixture rule based on the molar composition of the species is employed in this work to incorporate the most significant gas components. The parameters A, B and secondary electron emission coefficient ((γ_{se}) are obtained from literature, following [10] [6].

Particularly, in the presence of particles, the breakdown voltage significantly decreases. Therefore, the aim of this modelling study is to evaluate the breakdown voltage of the mixture gas, particles and finally deduce the arc-generating capability criteria. The modelling of particles as arcing source in the battery module or packs is not well researched as of now. Therefore, in this study we extracted the relevant modelling information from gas insulation systems of electronic components. The arcing behaviour in these devises are developed from quite some time. The potential and breakdown voltage of the particles are modelled from [11].

$$V_0 = E_0(d + r) + \frac{Q}{(4 \, \pi \, \varepsilon \, r)} \quad (9)$$

Where, V_0 is the potential of the particle and E_0 is the electrical field strength in the gas field, r is the radius of the particles and d is the distance to the electrode surface (earthed cathode, low voltage side) and Q is the electrical charge of the particle.

The breakdown field strength of the particles (E_{Bp}) is evaluated from experimentally fitted correlation [11].

$$E_{Bp} = 7.38 \, p \left\{1 + \frac{0.952}{\sqrt{p \, r}}\right\} \quad (10)$$

Where, p is the pressure and r is the radius of the particles. As per Eq. (10), as the particle radius increases electrical field strength decreases.

The breakdown voltage of the particle (V_{Bp}) is evaluated from:

$$V_{Bp} = E_{Bp} \, . \, d \qquad (11)$$

To summarise, the breakdown voltage in the gas medium is predicted using Eq. (8) and the breakdown voltage of the particles are predicted using Eq. (11). It is evident from these equations, that the break-down voltage depends on distance between the electrodes and pressure. Since the distance and pressure can change at every computational cell, the breakdown voltage may change accordingly. For e.g., in the case of venting gas ejection temperature and pressure field can be different from one computational cell to other computational cell and therefore breakdown voltage may vary accordingly.

3. RESULTS AND DISCUSSION

The results are first presented for simplified geometries and simplified battery modules as validation studies. Later, the evaluations are made on a real-world battery pack, and the corresponding results are presented at the end of this section. The results are arranged in the following order: flammability index of the gases, breakdown voltage of air, breakdown and arcing index with air and vent gas, breakdown voltage and arcing index with and without particles, particles ignited vent gas and finally the analysis of above models on real world battery pack.

Flammability of the vent gas mixture is simulated first in a simplified model where a vent gas mixture enters a domain filled with air. The vent gas mixture usually consists of some flammable hydrocarbons and inorganic components. Two different variants of the gaseous mixture are considered as the inlet boundary condition. The model conditions of these two simulations are shown in Figure 1.

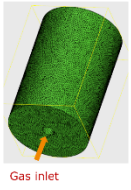

Model Cond.	Value
Velocity	5 m/s
Temperature	900 °C
Inlet species fractions	
CH4	0.33
CO	0.33
H2	0.34
C2H4	0.0

Model Cond.	Value
Velocity	5 m/s
Temperature	900 °C
Inlet species fractions	
CH4	0.25
CO	0.25
H2	0.25
C2H4	0.25

Figure 1: The geometry and the model conditions used for prediction of flammability limits of vent gas mixture.

Figure 2 describes the mixture flammability index and the pure component flammability index (for species CH4) respectively. As seen the flammable region is different for the two scenarios. The mixture flammability index takes into account all the flammable gases in the system according to Le Chatelier's principle as described in the previous Section 3. The flammable region in this case is slightly narrower but much wider making it as the bigger flammable region. In the case of pure component flammability, the fat region where CH_4 cannot burn is shown with 2.0 magnitude in the scale (see Figure 2 (c))

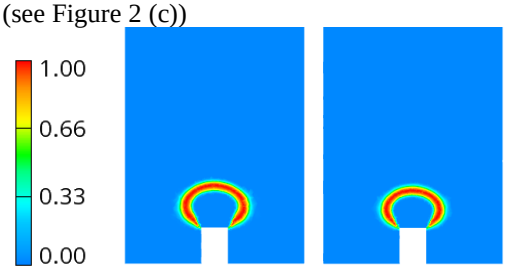

(a) Vent gas mixture flammability

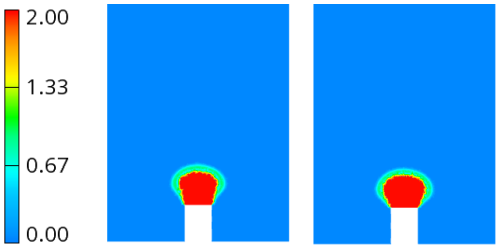

(b) Pure component flammability

Figure 2: Flammability index [-] evaluated based on

(a) mixture composition and

(b) pure component, the magnitude 2 in this case is a fat region representing no flammability.

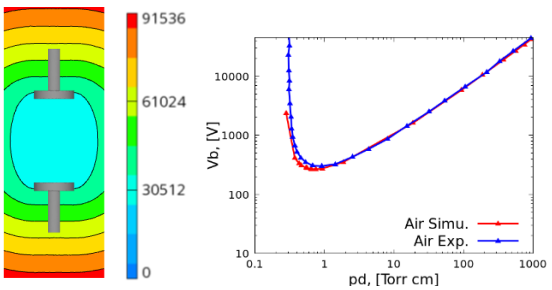

(a) (b)

Figure 3: (a) Breakdown voltage (V) between two parallel plate electrodes and

(b) validation of Paschen's curve for air

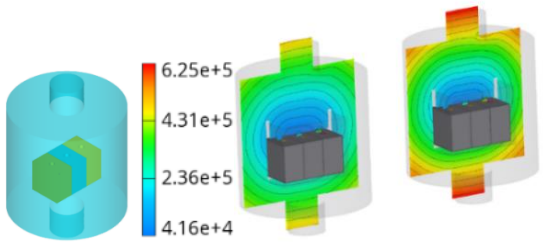

(a) (b) (c)

Figure 4: Breakdown voltage (V) evaluation in

(a) a simplified battery module with 3 prismatic cells (5 cm x 5 cm x 3 cm) placed in a cylindrical box (17 cm x 17 cm) at atmospheric pressure

(b) breakdown voltage venting gas mixture as medium

(c) breakdown voltage with air as medium

The quantitative evaluations are provided for electrode distances, breakdown voltage, critical distances and thus finally estimate the arc-generating capability. The implementation is first validated within a simple geometry where two electrodes are placed 1 cm apart within air medium. The contours of breakdown voltage and the comparisons with the experimental data of the Paschen's curve is shown in Figure 3 (a) and (b) respectively. The simulation data and the published data match well as seen in this figure. The current work also considers the original gas medium with its constituent species surrounding the module and pack instead of assuming air, shown in Figure 4. Considering the wide range of possible vent gases and their compositions, a methodology is developed to incorporate these mixtures in the evaluation of the overall breakdown voltage. This brings a more accurate description of the battery systems as the gas composition changes during a venting event which further brings down the breakdown voltage. Any decision made solely considering air as working medium poses serious consequences on the safety as seen in Figure 4. The breakdown voltage is approximately 30% lower with vent gas composition (see Figure 4 (b)) compared to air (see Figure 4 (c)) as the working medium. The breakdown voltage is lower near to the electrode surfaces (battery module) and increases away from the surfaces.

In addition, the effect of particles on the breakdown voltage is studied first in a simplified model and later in with the complete battery pack. For this purpose, as depicted in Figure 5, a setup with two electrodes separated by few mm of distance and as medium air is used. Conductive particles (copper particles) are introduced in varying size ranges, diameter 10 µm - 1000 µm. The total accumulated mass of the introduced particles is around 10 g. The voltage drop between these two electrodes is fixed for all the simulations at 1500 V. Electrical field strength, potential of the particle (*Vo*), breakdown field strength (*Eb*), breakdown voltage (*Vb*), and the arc generating capability (arc index) is presented in the following paragraph.

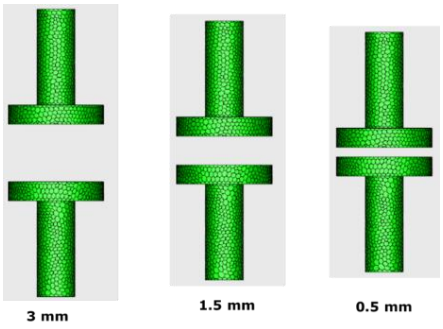

Figure 5: Two parallel electrodes separated by 3mm, 1.5 mm and 0.5 mm

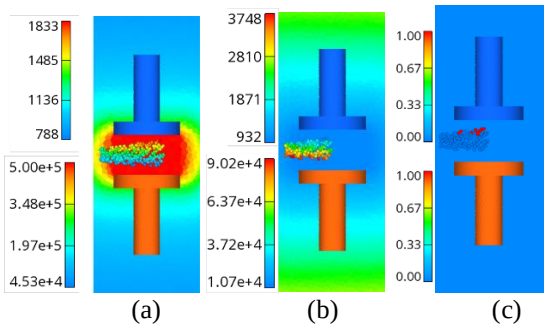

(a) (b) (c)

(i). for 1000 µm Particles & Gap Size 3 mm

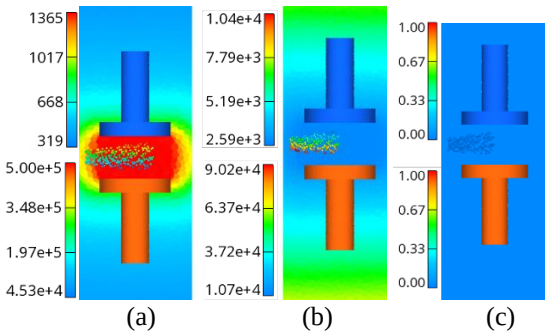

(a) (b) (c)

(ii). for 60 µm Particles & Gap Size 3 mm

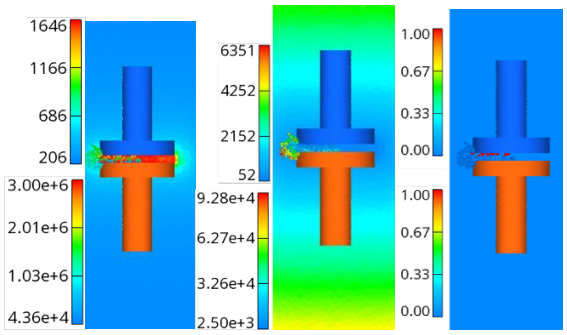

(a) (b) (c)

(iii). for 60 µm Particles & Gap Size 0.5 mm

Figure 6: For three different cases,
(i) Contour plots of potential of particles [V], electrical field strength in the gas medium [V/m],
(ii) Breakdown voltage [V] of both particles and gas medium,
(iii) Arc index [-] in the gas and as well as with the particles

Figure 6 presents the contour plots of potential of the particles (a), electrical field strength in the gas medium (a), breakdown voltage (b), and (c) arc index in gas medium as well as with the particles. The simulations are performed with a wide range of particle diameters and varying distances between the electrodes as depicted in Fig. 5 & 6 (i)-(iii). The results are presented only for the three test cases for the brevity of the manuscript. As seen in this figure, the breakdown voltage is greatly reduced with particles to a few hundred volts from few thousand volts when compared to the vent gas mixture. As depicted, the particle size and the distance between the electrodes greatly influences the breakdown voltage and the arcing probability. At a given distance of 3 mm particles with 1000 μm, few particles are prone to cause arcing (see Figure 6 (i)). Keeping the distance intact at 3 mm particles but reducing the particle diameter to 60 μm does not cause arcing (see Figure 6 (ii)). Keeping the particle diameter intact, i.e., at 60 μm, reducing the distance between the electrodes to 0.5 mm also increased the arc formation risks (see Fig. 6 (iii)). As the distance is reduced to 0.5 mm, the breakdown voltage greatly reduces, and some particles are prone to arcing. In these figures, arc-generating capability is shown in Fig. 6 (c) for cases (i)-(iii). For particles and gas with arc-generating capability one are prone to cause arcing and arc-generating capability zero does not cause arcing.

Particle ignited vent gas models are studied in a simplified battery module as shown in Figure 7. Two prismatic cells are placed in a casing containing air. A methane skeleton mechanism containing 19 species is considered for modelling the combustion in this case. Vent gas with CH4, CO, H2 and CO2 enters the module domain in the molar ratios 0.35, 0.3, 0.2 and 0.1 respectively where pure air is filled. Hot aluminum particles (900°C) ignite the vent gas released from the battery due to the presence of available O2 in the battery module.

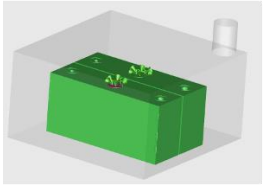

Figure 7: (a) Simplified battery module with two prismatic cells and surrounded by air medium.

The composition of the exerted methane, hot ejected particles, and subsequent ignition of the vent gas in the presence of hot particles is shown in Figure 8 and Figure 9 at two different time steps. The combustion starts at the periphery of the vent gas jet and propagates through the domain as the oxygen availability is present. As seen in Figure 9 (a), as the particles are ejected from the battery cell, the temperature immediately rises due to combustion reaction in the presence of hot particles. These particles act as sparks for starting the combustion process. The combustion further progresses in the domain as seen in Figure 9 (b).

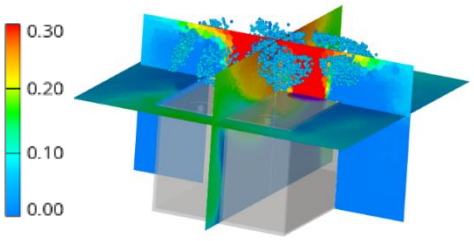

(a) Time = 0.52 s

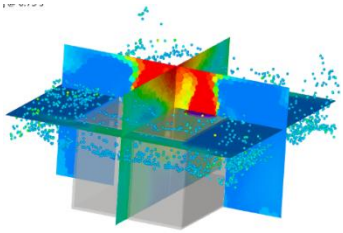

(b) Time = 0.75 s

Figure 8: Mass fraction of methane (-) at two different time steps in the battery module. The ignition starts as soon as the hot particles are ejected from the battery material

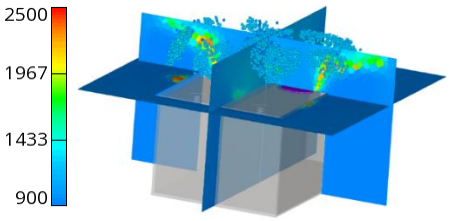

(a) Time = 0.52 s

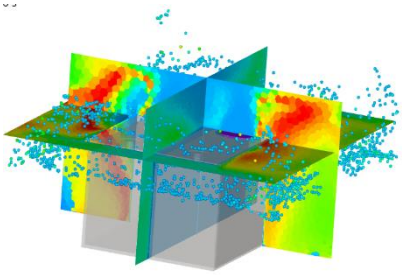

(b) Time = 0.75 s

Figure 9: Temperature (K) contours at two different time steps in the battery module. The ignition starts as soon as the hot particles are ejected from the battery material.

3.1 Description of battery pack under consideration

To evaluate the effects introduced in the previous chapter in a combined manner, a generic battery pack layout was used. The overall dimensions are 170 mm x 1270 mm x 830 mm. Separate details like screws, connector parts, as well as overall irrelevant super components (e.g.: the power converters) have been removed from the CAD model. Usually, battery packs used in the automotive industry do have some sort of liquid cooling. This has also been removed in this specific case.

Figure 10 shows an isometric view of the battery pack to the left and one selected battery module to the right. The whole battery pack consists of 12 battery modules assembled in a double-T-structure. Each battery module consists of 12 prismatic cells connected in series as can be seen in the figure.

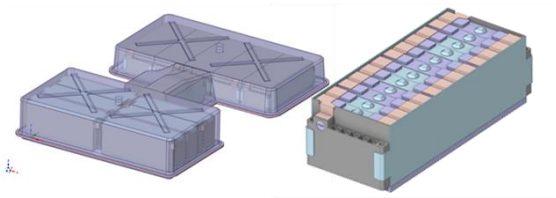

Figure 10: Battery Pack under investigation (left) and one battery module (right)

Components for a conjugate heat transfer simulation that have been retained in the pack are stated in Annex 1. Conductive and Convective heat transfer between all participating domains and media is considered. Radiative heat transfer is not considered. The inner cell material consisting of anode, cathode and electrolyte and the separator has been modelled as a lumped, single material. For thermal runaway considerations this is usually enough. The most important material property when it comes to thermal propagation (the heat spread from battery cell to battery cell in the case of thermal runaway) is the thermal conductivity. For the lumped battery cell, it has been assumed with anisotropic behavior. A list of the material properties can be seen in the table provided in Annex-I.

3.2 Description of thermal runaway modelling

A three-dimensional mesh of roughly 50 million polyhedral cells with sizes between 0.5 and 6 mm is used. The CFD simulation that is carried out is a fully coupled conjugate heat transfer simulation between all the domains mentioned in the previous chapter. Thermal runaway is a multi-phenomenon problem and therefore needs different aspects to be covered. The crucial to be evaluated modelling parts are described in the previous chapters. However, the other important effects are described here therefore the following sectors provide an overview of the model defects during thermal runaway. For the sake of simplicity, the chapters are kept short further information can be found in other papers of the authors [19, 20].

Battery cell heat release

The heat release in the battery cell is mainly characterized by electrochemical reactions, both endothermal (e.g., electrolyte vaporization) and exothermal (decomposition of cathode and anode). It can either be gathered from experiments in ARC reactors, as described by [21], or using chemical modelling, as described in [22–24]. For the sake of simplicity, a curve from AVL's benchmark data, that is appropriate for the battery cells under consideration is taken.

Venting

As the battery active materials undergo physico-chemical transformation (for e.g., SEI decomposition or the hot electrolyte vaporization), the pressure in the battery cell rises and is released either by ripping open the shell (pouch cells), or by exiting through a defined venting port (prismatic and cylindrical cells). The venting mass flow, temperature and species composition can either be gained from testbed data, as described by Golubkov et al. [25], or using a modelling approach like [26]. Within the context of this study, AVL's benchmark data, that is appropriate for the considered cell type, is taken.

Melting

The material properties of meltable parts, as well as the enthalpy of fusion, are taken into consideration for the melting of the material. If the enthalpy of fusion, in combination with start and end temperatures for melting, matches the energy in the meltable part, the solid part is removed, and airflow can pass through.

Burst discs

For the battery module under consideration one burst disc is used. A switchable boundary condition, turning from a wall when the burst disc is closed to a defined outlet pressure when the burst disc is opened, is used. The opening pressure difference is set to 300 mbar.

Particles

Particles are modelled using a Lagrangian description for the particle motion. Coupling of energy, momentum and turbulence exchange with

the surrounding gas phase is considered. Specific submodels are used for the drag law and evaporation. The secondary breakup of particles is not modelled within this study. The initial particle size distribution is constant.

3.3 Description of use case and simulation setup

A certain use case must be chosen to start the thermal runaway and observe its consequences on battery pack level. In this case the back of the pack, where these cells sit upright, has been considered one of the more dangerous use cases. This is due to the fact that the vent gas as well as the subsequent particles directly impinge on the battery pack housing. The following figure shows a top-down view of the battery pack and the initial cell being triggered for thermal runaway. The 12 battery modules are highlighted with respective numbers. This numbering system will be used throughout the paper especially in the interpretation of results.

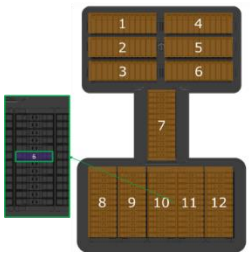

Figure 11: Top down view of the battery pack with triggered battery cell (cell 6 in module 11)

To start the thermal runaway in the simulation cell 6 in battery module 11 is set to an initial temperature of 160 [°C]. All other parts, including the surrounding air are set to 20 [°C]. Based on the cell's local temperature, a certain amount of heat is introduced to heat up the battery cell.

Once the average battery cell temperature reaches the venting temperature, vent gas with a time dependent venting volume, venting temperature and species composition is released in the defined "venting ports". During the venting event, also particles are released at the venting ports. Solid particle matter is ejected together with vent gas at the two venting outlets at the back of the battery pack as indicated in figure 2.

Total mass of solid particles and mass fractions of solid particle material is set to be similar to the results of the measurements from [27], where solid particles were analyzed after thermal runaway of a prismatic cell.

The module covers are treated as meltable solid parts that start to melt at the melting temperature of the applied materials.

Initial time step is set to 0.01 s with an adaptive time step control, adjusting time steps according to critical physical states like predefined critical gas mass flow or burst disc state (f.e. open/closed). Gas species considered for the vent gas are CH_4, H_2 and CO with mole fractions set to 0.3, 0.4, 0.3, respectively. The validity of the modelling approach has been demonstrated in [19] where thermal propagation times and burst disc opening timings have been compared to measurement data. Therefore, the following section will be used to analyze the results with respect to the risk of flammability and arcing. Figure 12 shows the venting of cell 6 in module 11 after about 0.5 s after thermal runaway was triggered in the cell. The image is a zoomed in, isometric view on the battery cell. One can see the battery cells in grey, the busbars in orange. The meltable module covers are only shown in the left part of the image to not obscure the readers view – they are shown as golden, opaque surfaces.

3.4 Evaluation of flammability and particle ignition

The temperature is shown in the first image, the flammability index is shown in the second image. One can see that the gas jet exits with a quite high temperature. It impinges on the meltable covers as they are not molten yet. Due to the fact the vent gas itself has no oxygen in it, the flammability index in the gas jet is zero. Only on the contour of the jet the flammable gases (H2, CH4, CO) mix with oxygen and form a combustible mixture. Here the flammability index has positive values. A correlation could now be made with the solid particles in the vicinity to evaluate possible ignition spots.

3.5 Evaluation of arcing

In the following figure the reader can see the breakdown voltage of the gas mixture – here the view is again an isometric view on battery module 11. The cut-plane shows the breakdown voltage of the gas mixture which is calculated using Paschen's law as described in the earlier chapters. The corresponding values can be seen in the range on the top of the image. The values are still in the range of 10.000 V and more, which is too high for arc formation. This was also observed in the work of [8]. The flammable vent gases reduce the breakdown voltage, but it is still too high to cause arcing in battery packs where voltages of the High Voltage (HV) carriers are at about 800 V. However, in the image also the breakdown voltage of particles can be observed. The range is stated on the lower part of the image. The particles impinged on the meltable module covers and bounced back on the busbars as shown in the image. Here they are now close to the current carrying parts and their breakdown voltage is in the range 100-1000 V, which makes the probability for arcing very high.

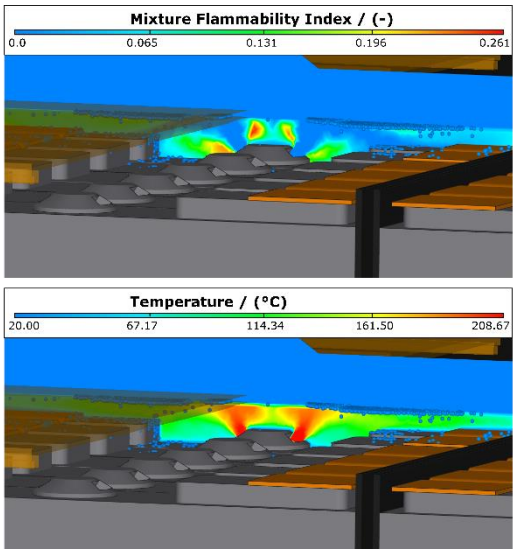

Figure 12: Isometric view of battery cell 6 in module 11 during thermal runaway (top: Temperarture, bottom: Flammability Index)

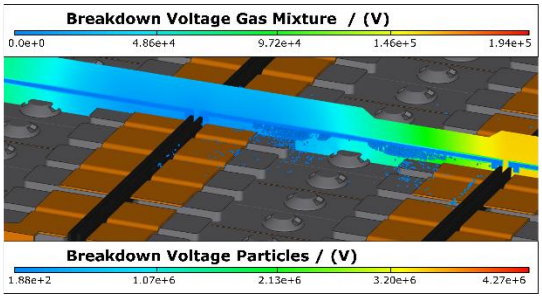

Figure 13: Breakdown Voltage of air (cutplane) and for particles (shown on particle spheres) for the thermal runaway of cell 6

4. SUMMARY

Current study focuses on several predictive models for battery safety and hazard prediction. Flammability, breakdown voltage, arcing are modelled and simulated by considering several possible vent gas species and the solid particles. The developed models are first investigated on simple representative battery module and later, on real life battery pack. The simulation results on the simplified geometries verify the qualitative behaviour of flammability, breakdown voltage and arcing on the system variables. The pack level simulation highlights the applicability of the developed models on complex geometries and provides qualitative and quantitive analysis of the safety operating conditions in the battery packs. Finally, a methodology is presented for particle initiated combustion of the venting gas mixture by considering a reduced skeleton gaseous combustion mechanism (from GRI). The venting gas combustion with particles as ignition source and the flame propagation in the battery packs highlights the modelling capabilities in understanding the possible hazards in the battery packs. The new, advanced features like arcing related quantities for the vent gas and particles can give temporal and spatial view on possible hot spots related to arc formation in the battery pack. Further efforts will focus on correlations between the electrical circuit and breakdown voltage(s) to calculate the full electromagnetics in the battery pack

References

[1] Bugryniec PJ, Resendiz EG, Nwophoke SM, Khanna S, James C, Brown SF. Review of gas emissions from lithium-ion battery thermal runaway failure — Considering toxic and flammable compounds. J Energy Storage 2024;87. https://doi.org/10.1016/j.est.2024.111288.

[2] Baird AR, Archibald EJ, Marr KC, Ezekoye OA. Explosion hazards from lithium-ion battery vent gas. J Power Sources 2020;446. https://doi.org/10.1016/j.jpowsour.2019.227257.

[3] Zlochower IA, Green GM. The limiting oxygen concentration and flammability limits of gases and gas mixtures. J Loss Prev Process Ind 2009;22:499–505. https://doi.org/10.1016/j.jlp.2009.03.006.

[4] Mashuga C V, Crow1 DA. Derivation of Le Chatelier's Mixing Rde for Flammable Limits. n.d.

[5] Kondo S, Takizawa K, Takahashi A, Tokuhashi K, Sekiya A. A study on flammability limits of fuel mixtures. J Hazard Mater 2008;155:440–8. https://doi.org/10.1016/j.jhazmat.2007.11.085.

[6] Marić D, Savić M, Sivoš J, Škoro N, Radmilović-Radjenović M, Malović G, et al. Gas breakdown and secondary electron yields. European Physical Journal D 2014;68. https://doi.org/10.1140/epjd/e2014-50090-x.

[7] Babrauskas V. Arc Breakdown in Air over Very Small Gap Distances. n.d.

[8] Ledinski T, Golubkov AW, Schweighofer O, Erker S. Arcing in Li-Ion Batteries. Batteries 2023;9. https://doi.org/10.3390/batteries9110540.

[9] Massarczyk R, Chu P, Dugger C, Elliott SR, Rielage K, Xu W. Paschen's law studies in cold gases. Journal of Instrumentation 2017;12. https://doi.org/10.1088/1748-0221/12/06/P06019.

[10] Gudmundsson JT, Lundin D. Introduction to magnetron sputtering. High Power Impulse Magnetron Sputtering: Fundamentals, Technologies, Challenges and Applications, Elsevier; 2019, p. 1–48. https://doi.org/10.1016/B978-0-12-812454-3.00006-1.

[11] Hara M, Akazaki M. A method for prediction of gaseous discharge threshold voltage in the presence of a conducting particle. J Electrostat 1976;2:223.
[12] Hara M. Analysis of microdischarge threshold conditions between a conducting sphere and plane. J Electrostat 1982;13:105–18.
[13] Sakai K-I, Abella DL, Suehiro J, Hayashi N, Hara M. Mode of Free-Conducting Particle Motion and Particle-Triggered Breakdown Mechanism in Non-uniform Field Gaps. 2000.
[14] Gongquan Wang, Depeng Kong, Ping Ping, Jennifer Wen, Xiaoqin He, Hengle Zhao, et al. Revealing particle venting of lithium-ion batteries during thermal runaway: A multi-scale model toward multiphase process. ETransportation 2023;16.
[15] Wang Q, Ping P, Zhao X, Chu G, Sun J, Chen C. Thermal runaway caused fire and explosion of lithium ion battery. J Power Sources 2012;208:210–24. https://doi.org/10.1016/j.jpowsour.2012.02.038.
[16] Ferziger JH, Peric M. Computational methods for fluid mechanics. vol. 5. 2002.
[17] Schellander D, Schneiderbauer S, Pirker S. Numerical study of dilute and dense poly-dispersed gas-solid two-phase flows using an Eulerian and Lagrangian hybrid model. Chem Eng Sci 2013.
[18] http://combustion.berkeley.edu/gri-mech/ n.d.
[19] Maier G, Eder L, Schneider J, Suzzi D. Numerische Untersuchung des Thermal Runaway in Lithium-Ionen Batteriesystemen. n.d.
[20] Fritz M, Lucas E, Jürgen S, Thomann M. Modelling and Evaluation of Venting Particles during Battery Thermal Runaway Simulation. KSAE 2022 Annual Autumn Conference & Exhibitio, The Korean Society Of Automotive Engineers; 2022, p. 1684–93.
[21] Essl C, Golubkov AW, Gasser E, Nachtnebel M, Zankel A, Ewert E, et al. Comprehensive hazard analysis of failing automotive lithium-ion batteries in overtemperature experiments. Batteries 2020;6. https://doi.org/10.3390/batteries6020030.
[22] Ren D, Liu X, Feng X, Lu L, Ouyang M, Li J, et al. Model-based thermal runaway prediction of lithium-ion batteries from kinetics analysis of cell components. Appl Energy 2018;228:633–44. https://doi.org/10.1016/j.apenergy.2018.06.126.
[23] García A, Monsalve-Serrano J, Lago Sari R, Fogué Robles Á. Numerical analysis of kinetic mechanisms for battery thermal runaway prediction in lithium-ion batteries. International Journal of Engine Research 2022;23:1691–707. https://doi.org/10.1177/14680874211029902.
[24] Kim GH, Pesaran A, Spotnitz R. A three-dimensional thermal abuse model for lithium-ion cells. J Power Sources 2007;170:476–89. https://doi.org/10.1016/j.jpowsour.2007.04.018.
[25] Golubkov AW, Fuchs D, Wagner J, Wiltsche H, Stangl C, Fauler G, et al. Thermal-runaway experiments on consumer Li-ion batteries with metal-oxide and olivin-type cathodes. RSC Adv 2014;4:3633–42. https://doi.org/10.1039/c3ra45748f.
[26] Coman PT, Rayman S, White RE. A lumped model of venting during thermal runaway in a cylindrical Lithium Cobalt Oxide lithium-ion cell. J Power Sources 2016;307:56–62. https://doi.org/10.1016/j.jpowsour.2015.12.088.
[27] Zhang Y, Wang H, Li W, Li C, Ouyang M. Size distribution and elemental composition of vent particles from abused prismatic Ni-rich automotive lithium-ion batteries. J Energy Storage 2019;26. https://doi.org/10.1016/j.est.2019.100991.

Annex-I

Table 1: Used material properties for the battery pack CFD simulation

Group	Material	Average Density [kg/m³]	Specific heat capacity [J/kgK]	Thermal Conductivity [W/mK]
Inner Cells	Cell Material	2400	1500	33 / 0.7 / 33
Cell Shells	Aluminium	2700	Table	236
Spacer	Plastic	1200	1800	0.3
Endplates	Aluminium	2700	Table	236
Sidplates	Aluminium	2700	Table	236
Baseplates	Aluminium	2700	Table	236
Covers	Plastic	1200	1800	0.3
Busbars	Copper	8960	Table	401
Lower Housing	Steel	7700	Table	Table
Upper Housing	Steel	7700	Table	Table
Sealing Lip	Plastic	1200	1800	0.3
Inner Air	Air (compressible)	Table	Table	Table